

Modeling of Fate and Transport of Co-injection of H₂S with CO₂ in Deep Saline Formations

Wei Zhang¹, Tianfu Xu², Yilian Li¹

1. School of Environmental studies, China University of Geosciences, Wuhan, Hubei 430074, China

2. Earth Sciences Division, Lawrence Berkeley National Laboratory, University of California, Berkeley, CA 94720, USA

Abstract: The geological storage of CO₂ in deep saline formations is increasing seen as a viable strategy to reduce the release of greenhouse gases into the atmosphere. However, costs of capture and compression of CO₂ from industrial waste streams containing small quantities of sulfur and nitrogen compounds such as SO₂, H₂S and N₂ are very expensive. Therefore, studies on the co-injection of CO₂ containing other acid gases from industrial emissions are very important. In this paper, numerical simulations were performed to study the co-injection of H₂S with CO₂ in sandstone and carbonate formations. Results indicate that the preferential dissolution of H₂S gas (compared with CO₂ gas) into formation water results in the delayed breakthrough of H₂S gas. Co-injection of H₂S results in the precipitation of pyrite through interactions between the dissolved H₂S and Fe²⁺ from the dissolution of Fe-bearing minerals. Additional injection of H₂S reduces the capabilities for solubility and mineral trappings of CO₂ compared to the CO₂ only case. In comparison to the sandstone (siliciclastic) formation, the carbonate formation is **less** favorable to the mineral sequestration of CO₂. Different from CO₂ mineral trapping, the presence of Fe-bearing siliciclastic and/or carbonate is more favorable to the H₂S mineral trapping.

1 Introduction

Global emissions of greenhouse gases (GHG) especially carbon dioxide (CO₂) have increased rapidly and led to global climate change and ocean acidification with severe consequences for ecosystems and for human society [Holloway, 2001; West *et al.*, 2005]. Thus, reducing the concentration of CO₂ in the atmosphere is very important to the mitigation of global climate change. Currently, research on CO₂ geological storage as a possible method for reducing the emission of CO₂ from industrial point sources is being extensively carried out [Gentzis, 2000; Holloway, 2005; Gough, 2008]. The main geologic formations include depleted or depleting oil and gas reservoirs, un-mineable coal seams, and deep saline formations [Bachu *et al.*, 1994; Hitchon *et al.*, 1999]. Injecting CO₂ into saline formations in sedimentary basins is one of the most promising methods of CO₂ geological storage for the long-term sequestration of the gas. This is because saline formations are ubiquitous to sedimentary basins [Hitchon *et al.*, 1999; Gunter *et al.*, 2000; Izgec *et al.*, 2008], they have enough capacity to store large amounts of CO₂ from anthropogenic emissions, and there are short distances between most large CO₂ point sources and saline formations, which can minimize CO₂ transportation costs [Soong *et al.*, 2004; Allen *et al.*, 2005; Zerai *et al.*, 2006].

The fate of minor quantities of sulfur and nitrogen compounds during combustion or gasification of coal is of considerable interest, as their release into the atmosphere leads to the formation of urban ozone and acid rain, the destruction of stratospheric ozone, and global warming. Coal also contains many trace elements that are potentially hazardous to human health and the environment, such as mercury and arsenic, and their release into the atmosphere is restricted under the Clean Air Act Amendments (CAAA) of 1990. Studies indicated that costs of capture and compression of CO₂ from flue gas or a coal gasification process are very high,

accounting for 75% of the total cost of a geological storage process [Knauss *et al.*, 2005]. Therefore it may be economically advantageous to sequester/store CO₂ with these constituents in deep geological formations [Knauss *et al.*, 2005; Bachu *et al.*, 2009a; Ellis *et al.*, 2009; Xiao *et al.*, 2009; Crandell *et al.*, 2010]. In this study, we evaluate the co-injection of hydrogen sulphide (H₂S) with CO₂.

In order to reduce emissions of produced H₂S and CO₂ as byproducts of sour gas processing, a total of more than 40 active acid-gas injection projects were performed in the Alberta Basin of Canada to the end of 2003 [Bachu and Gunter, 2005]. The acid gas can be injected as solution or dense fluid (liquid or supercritical). The injected gas composition varies from 83% H₂S and 14% CO₂ to 2% H₂S and 95% CO₂ for different storage sites [Bachu *et al.*, 2005]. Since the first acid-gas injection operation in a depleted sandstone oil reservoir on the outskirts of Edmonton began in 1989, no leakage or other safety problems have been reported [Bachu and Gunter, 2004; Machel, 2005]. At the end of 2003, a total of about 2 Mt H₂S and 2.5 Mt CO₂ were injected in deep saline formations, and depleted oil or gas reservoirs, for all storage sites in western Canada, at average rates that vary between 1×10^3 and 500×10^3 m³/day [Bachu and Gunter, 2005; Bachu *et al.*, 2005]. The success of these acid-gas injection projects in Canada and the U.S.A [Bachu *et al.*, 2009b] indicate that the co-injection of H₂S and CO₂ in geological media is a mature and safe technology.

The acid gases from natural gas production contain 2-84 vol. % H₂S, but most coals contain no more than 5 wt. % sulfur. Therefore, the concentration of H₂S in CO₂ from the integrated gas combined cycle (IGCC) plants is unlikely to exceed 1.5 vol. % [Gunter *et al.*, 2000; Xu *et al.*, 2007].

In order to better understand the multiphase fluid transport and geochemical reactions during

the co-injection process of acid gases. Some laboratory experiments have been conducted for a short time. *Bachu et al.* [2009a; 2009b], and *Bachu and Bennion* [2009] used a **series** of static and dynamic experiments to investigate the effects of gas concentration and in-situ conditions of pressure, temperature and water salinity on the partitioning of CO₂ and H₂S. Experimental results showed that the higher solubility of H₂S than that of CO₂ results in suppressed H₂S concentrations at the leading edge of the breakthrough gas phase. They also performed 1-D numerical simulations to study the effect of flow conditions such as gas solubility, medium absolute and relative permeabilities, dispersion, mobility and displacement direction on the time of CO₂ and H₂S breakthrough. In these studies, however, water-gas-rock chemical interactions are not addressed. The chemical processes are very important for the long-term fate and transport of injected acid gases, because these interactions may cause major changes in the rock structure and chemical composition of the storage formation. *Gunter et al.* [2005] performed autoclave batch experiments to study the reaction of siderite with acid gas (CO₂ and H₂S) at the conditions of 5.15 bars and 54°C for 14 days. Analysis results of the reaction products showed that the precipitated sulfide mineral during the experiment is pyrite.

On the other hand, many modeling studies have concentrated on chemical processes induced by the co-injection of H₂S with CO₂. *Knauss et al.* [2005] used a 1-D reactive transport simulation and found that the additional injection of dissolved H₂S with CO₂ as an aqueous phase does not have a significant impact on the water-rock interaction compared to the CO₂ only case. *Gunter et al.* [2000] used a batch geochemical model to study the interaction of industrial waste streams comprising CO₂ and H₂S with the minerals in typical carbonate and sandstone (siliciclastic) formations from the Alberta Basin, Canada. Their simulation results indicated that decrease in pH caused by dissolution of injected H₂S results in the dissolution of siderite which provides Fe²⁺ to

the precipitation of pyrrhotite. *Xu et al.* [2007] developed a 1-D radial flow model for modeling of co-injection of dissolved H₂S with gaseous CO₂ in a sandstone formation. Their simulation results showed that the co-injection, compared to the CO₂ injection only, does not significantly affect pH distribution, mineral alteration, and CO₂ mineral trapping. The main difference is precipitation of pyrite in the co-injection case.

Some of previous reactive transport modeling [e.g., *Xu et al.*, 2007; *Xiao et al.*, 2009] **are** limited in that only CO₂ can be injected in the gaseous state. Therefore, co-injection of brines carrying dissolved H₂S was used for expediency. The consequences of this artifact on the model results, especially in relation to CO₂ sequestration, are relatively minor because injection occurs only in the early time, much shorter than the simulation time (in the order of 1,000 years).

In this paper, fluid flow modeling capabilities for injection of anhydrous supercritical CO₂ containing H₂S gas are employed due to the improvement of a version of TOUGHREACT (see more details in Section 2.1). We performed two-dimensional (2-D) radial flow modeling to study co-injection of H₂S with CO₂ in sandstone and carbonate formations. The 2-D radial flow model used here allows us to study buoyancy forces that would tend to drive the gas mixture towards the top of the formation, which cannot be demonstrated by the previous 1-D well models [e.g., *Xu et al.*, 2007]. Compared to *Xu et al.* [2007], this paper is a significant step forward on modeling of injection of H₂S with CO₂ and subsequent fate and transport. The simulation results can be used to evaluate the behavior and effect of impurity-H₂S in the CO₂ stream and their performance during the injection and storage period.

2 Numerical approaches

2.1 Numerical tool

The present simulations employed the non-isothermal multiphase reactive geochemical transport code TOUGHREACT [Xu and Pruess, 2001; Xu et al., 2006], which is developed by introducing reactive chemistry into the multiphase fluid and heat flow code TOUGH2 [Pruess et al., 1999, 2004]. An improved version [Battistelli, 2008] of the TMVOC simulator [Pruess and Battistelli, 2002] was linked to TOUGHREACT, resulting in an acid gas injection simulator (Xu, unpublished). TMVOC models the migration of three-phase multi-component inorganic gases and hydrocarbons mixtures for environmental applications. The improved TMVOC can simulate the two-phase behaviour of sodium chloride dominated brines in equilibrium with a non aqueous phase made up of inorganic gases, such as CO₂, H₂S and N₂ and hydrocarbons (alkanes up to decane, benzene, toluene, ethylbenzene and xylenes (BTEX), and pseudo-components). It can then be used to model injection of acid gas mixtures in saline formations, and account for the presence of additional gaseous species in the injected CO₂, such as contaminants like H₂S or N₂.

The numerical method for solving fluid flow and chemical transport is based on an integral finite difference (IFD) method for space-discretization [Narasimhan and Whitherspoon, 1976]. The IFD method provides flexible discretization of geologic media by allowing the use of irregular grids, which is well suited for simulation of flow, transport, and fluid-rock interaction in heterogeneous and fracture rock systems with varying petrology. For regular grids, the IFD method is equivalent to the Conventional Finite Difference method. An implicit time-weighting scheme is used for the flow, transport and kinetic geochemical equations. TOUGHREACT uses a sequential iteration approach similar to that described by Yeh and Tripathi [1991]. After solution of the flow equations, the velocities and saturations of the aqueous phase are used for aqueous

chemical transport simulation. Chemical transport is then solved on a component basis. Resulting concentration obtained from the transport and CO₂ and H₂S gas pressures in the multiphase flow calculation are substituted into the chemical reaction model. The system of chemical reaction equations is solved on a grid-block basis by Newton-Raphson iteration. The program can be applied to one-, two-, or three-dimensional porous and fractured media with physical and chemical heterogeneity. It can accommodate any number of chemical species present in the liquid, gas and solid phases. A wide range of subsurface thermo-physico-chemical processes are considered under various thermohydrological and geochemical conditions such as pressure, temperature, ionic strength, pH and Eh. Changes in porosity and permeability due to mineral dissolution and precipitation can modify fluid flow. Feedback between flow and chemistry can be considered in this model. Porosity changes are calculated from volume changes due to mineral dissolution and precipitation. Permeability changes can then be evaluated by consideration of several alternative models describing the porosity-permeability relationship, including a simple grain model of Kozeny-Carman, as used in the present study.

2.2 Model setup

Much specific and detailed information is required to assess the feasibility of the acid-gas injection and to develop engineering designs for the injection systems. Before conducting site-specific investigations, general features and issues relating to the injected formation should be explored. This can be done by extracting the site-specific features and representing characteristics. Increases in geological and geometric complexities can increase the difficulty of identifying the dominant geochemical processes. Therefore, a simple two-dimensional (2-D) radial well model was used in this study. The 2-D model was a homogeneous formation of 50 m thickness with a

cylindrical geometrical configuration (Figure 1). In the vertical direction, 25 model layers were used with a constant spacing of 2 m. In the horizontal direction, a radial distance of 100 km was modeled with a radial grid spacing that increases gradually away from the injection well. A total of 50 radial grid elements were used. The volume of the outer grid element is specified a large value of 10^{30} m^3 , representing an infinitive lateral boundary. CO₂ only or CO₂ containing H₂S injection was applied at the bottom portion of the well (the thickness of the injection portion is 20 m). Injection of acid gases was applied for a period of 10 years, using a CO₂ injection rate of 2 kg/s (~0.063 Mt/yr) for the CO₂ only case, or using a CO₂ injection rate of 1.9 kg/s (~0.06 Mt/yr) and a H₂S injection rate of 0.1 kg/s (~0.003 Mt/yr) for the co-injection case. The fluid flow and geochemical transport simulation was run for a period of 500 years, which may be a relevant time scale of interests for geological sequestration of acid gases.

We used the same hydrogeological parameters as those used in the research in the Songliao Basin of China [Zhang *et al.*, 2009], which is listed in Table A.1 in Appendix A. Two types of (initial) mineralogical compositions (Table A.2 in Appendix A) were used, sandstone from Zhang *et al.* [2009] and carbonate from Zerai *et al.* [2006].

Prior to simulating reactive transport, a batch geochemical modeling of water-rock interaction was performed to generate an aqueous-phase chemical composition closely approaching the composition of a typical formation brine by equilibrating a 0.171 M (mol/kg H₂O) solution of sodium chloride in the presence of the primary minerals listed in Table A.2 with CO₂ gas pressure of 0.01 bar at a temperature of 50°C. We are primarily interested in the region affected by CO₂ injection. The uncertainty of background CO₂ pressure on simulation results should be very small for our objectives. A reasonably short simulation time (10 years in the present study) is needed to obtain a quasi-stable (or nearly steady-state) aqueous solution composition (Table A.3 in

Appendix A).

Dissolution and precipitation of minerals are considered under kinetic conditions. The rate laws used is presented in Appendix B. The kinetic parameters were taken from *Xu et al.* [2007] and *Zhang et al.* [2009], which is listed in Table C.1 in Appendix C. A temperature of 50°C was used, which may represent the temperature at a depth of about 1200 m, given a land surface temperature of 15°C and a geothermal gradient of 30°C/km.

2.3 Simulations

As shown in Table 1, a total of four groups of numerical simulations were performed with different combinations of injection scenario and rock type. The purpose is to investigate the effect of additional H₂S injected with CO₂ in different rock-types (e.g., sandstone and carbonate) on the geochemical changes (aqueous composition, and mineral dissolution and precipitation), fate and transport of injected CO₂ and H₂S gases.

3 Results and discussion

3.1 Sandstone formation

Figure 2 shows that CO₂ and H₂S gases (supercritical) injected at the bottom of the deep saline formation migrate upward rapidly by buoyancy forces. Mass fraction of CO₂ at the advancing gas front is higher (Figures 2a and 2b). The front of H₂S gas is behind that of CO₂ gas (Figures 2c and 2d). This is due to the preferential solubility of H₂S in formation water compared with that of CO₂, which induces the delayed breakthrough of H₂S gas, the separation between CO₂ and H₂S gases, and suppressed H₂S concentrations in formation water at the advancing gas front [Bachu *et al.*, 2009a, 2009b; Bachu and Bennion, 2009]. Figure 3 shows the spatial distribution of total dissolved sulfur (TDSu) and carbon (TDC) in the sandstone formation. There is a greater concentration of TDSu in the interior of the gas plume, corresponding to the higher H₂S mass fraction in the gas phase than that in the other region.

In order to better understand the relationship among the concentration of TDC and TDSu, the mass fraction of CO₂ and H₂S in the gas phase, and the partial pressure of CO₂ and H₂S, we plot their changes with time based on a point A in the model, which lies in the two-phase zone where CO₂ gas and aqueous phases coexist (see Figure 2b). Figure 4 reveals that when the injected CO₂ gas reaches the point A, the mass fraction of CO₂ in the gas phase is higher than that in the initial gases injected (0.95, namely the dash-dot-dot line in Figure 4a). The temporal evolution of mass fraction of CO₂ and H₂S indicates CO₂ reaches the point A faster than H₂S. This is due to the preferential dissolution of H₂S compared with CO₂.

Trends in concentrations of TDC in the CO₂ containing H₂S and CO₂ only cases, and TDSu in the co-injection case are generally similar to variations in partial pressures of CO₂ and H₂S. Trend in concentrations of TDC is opposite to that of TDSu after the gases reach this point. As expected

the concentration of TDC in the co-injection case is lower than that in the CO₂ alone case. These indicate again the preferential dissolution of H₂S gas reduces the potential and capacity for the dissolution of the injected CO₂ gas in formation water. However, with the decrease in TDS concentration caused by the decrease in H₂S partial pressure, the solubility of CO₂ in formation water will gradually increase.

Dissolution of CO₂ and H₂S lowered pH of formation water, then induced dissolution and precipitation of minerals. Chlorite (Mg_{2.5}Fe_{2.5}Al₂Si₃O₁₀(OH)₈) dissolves (Figure 5a), which supplies Fe²⁺ and Mg²⁺ for the precipitation of ankerite (CaMg_{0.3}Fe_{0.7}(CO₃)₂) (Figure 5b) and pyrite (FeS₂) (Figure 5c) for the case of CO₂ containing H₂S. Figure 6a shows cumulative CO₂ sequestered by carbonate precipitation (mineral trapping) in the sandstone formation. Precipitation of ankerite requires Ca²⁺ provided by dissolution of calcite (CaCO₃) (Figure 5d). In the case of co-injection of H₂S, pyrite precipitation occurs in the two-phase zone, and ankerite precipitation occurs in the aqueous phase zone. This is because the pH in the two-phase zone is lower than that in the aqueous phase zone (Figure 6b), and pyrite is stable under relatively low pH conditions.

Dissolution of chlorite in the CO₂ only case (Figure 7a) is similar to that in the CO₂ containing H₂S case (Figure 5a). Due to the amount of precipitated ankerite in the co-injection case (Figure 5b) is lower than that in the CO₂ only case (Figure 7b), the abundance of dissolved calcite in the former case (Figure 5d) is also lower than that in the later case (Figure 7c). In the CO₂ alone case, the CO₂ mineral trapping (Figure 7d) is greater than those in the CO₂ containing H₂S case. This is because the precipitation of pyrite suppresses the precipitation of Fe-bearing carbonate minerals such as ankerite.

Note that due to the mineral trapping of CO₂ is a slow process, there is no significant increase

in mineral trapping amount compared with the gas and solubility trapping mechanisms under the present mineralogical composition. Therefore, we only investigate changes in gas, and aqueous+solid phases for different cases, respectively. Temporal changes in fractions of injected CO₂ trapped in gas, and aqueous and solid phases obtained from cases of CO₂ containing H₂S and CO₂ only in sandstone formations (Figure 8) confirms that preferential dissolution of H₂S can suppress CO₂ dissolution.

The 1-D simulation results from *Xu et al.* [2007] indicated that additional injection of H₂S causes more pyrite precipitation than the CO₂ only case. And compared to the CO₂ alone case, precipitation of pyrite in the low-pH region for the case of H₂S co-injection reduces ankerite precipitation in this zone. These modeling results are in agreement with our 2-D study. However, due to constraints of the previous version of TOUGHREACT, the injected H₂S is assumed as aqueous phase. The acid gas injection simulator used in current study can model both CO₂ and H₂S in gaseous state. The higher solubility of H₂S gas in formation water than CO₂, affects the fate and transport of injected CO₂ and H₂S gases, including the delayed breakthrough of H₂S, the separation between the two gases, and suppressed H₂S concentrations in formation water at the advancing gas front. These were not be obtained from the study of *Xu et al.* [2007] because injected H₂S is in the aqueous phase. Compared to the previous 1-D model [e.g., *Knauss et al.*, 2005; *Xu et al.*, 2007; *Bachu and Bennion*, 2009; and *Bachu et al.*, 2009b], the current 2-D radial flow model allows us to study buoyancy forces that would tend to drive the gas mixture towards the top of the formation, to track transport and dissolution of CO₂ and H₂S at the front of the gas plume, to investigate variations of physical and chemical processes over vertical cross-section.

3.2 Carbonate formation

Figure 9a shows that decrease of H₂S amount in the gas phase for the carbonate (with siderite) formation is more significant than that for the sandstone formation. This is because dissolution of siderite available in carbonate (Figure 10a) is faster than that of chlorite available in sandstone, accelerating precipitation of pyrite (Figure 10b) and driving more H₂S dissolution (Figures 11a and 11b) into formation water. The predicted precipitation of pyrite is consistent with the experiment results reported by *Gunter et al.* [2005]. As expected, the decrease in TDSu concentration (Figures 12a and 12b) induced by the decrease in H₂S partial pressure should enhance the more CO₂ dissolution due to the increasing contact between CO₂ gas and formation water (Figures 11c and 11d). However, Figure 9b indicates that decrease in CO₂ gas in the carbonate formation is less than that in the sandstone formation. This is because dissolution of carbonates such as dolomite (Figure 10c) and siderite increases the concentration of total dissolved carbon in formation water, which can suppress the CO₂ dissolution. Some amounts of calcite precipitate (Figure 10d), and ankerite precipitation is limited.

Some typical carbonate formations do not have siderite. Therefore, we performed a sensitivity simulation to investigate the effect of co-injection of CO₂ containing H₂S in a no Fe-bearing carbonate formation. Figure 9a shows that dissolution of H₂S in the carbonate (without siderite) formation is much less than that in sandstone and carbonate formations. Temporal changes of H₂S gas in this case confirm again that dissolution of Fe-bearing minerals such as chlorite and siderite has a strong impact on reduction of H₂S in the gas phase because of formation of pyrite.

As expected, the significant decrease of H₂S amount in the gas phase for the carbonate (with siderite) formation should enhance CO₂ dissolution (compared to the carbonate case without siderite). However, temporal changes of CO₂ gas for two cases in carbonate formations do not

have a significant difference (Figure 9b). This should be because the siderite dissolution in the carbonate case provides Fe^{2+} to precipitation of pyrite, and increases the concentration of TDC in formation water, which can inhibit the dissolution of CO_2 gas. Changes in dolomite and calcite volume fractions (Figure 13) in this case are similar to the previous case with siderite (Figure 10).

The increased concentration of H^+ in aqueous phase induced by acid gas injection interacts with aluminosilicate and/or silicate minerals such as feldspars and clay minerals releasing cations such as Ca^{2+} , Mg^{2+} , and Fe^{2+} . The dissolved bicarbonate species reacts with these divalent cations to precipitate carbonate minerals, sequestering CO_2 permanently. Therefore, siliciclastic (sandstone) formations are more favorable for CO_2 mineral trapping than carbonate formations [Hitchon *et al.*, 1999; Gentsis, 2000]. This does not mean that carbonate formations are not suitable for the geological storage of CO_2 , but that the dominant trapping mechanisms in carbonate formations are solubility and hydrodynamic trappings [Zerai *et al.*, 2006].

However, if there are Fe-bearing siliciclastic and/or carbonate minerals occurred in primary minerals, sulfide minerals such as pyrite can precipitate in the sandstone and carbonate formations, increasing mineral trapping of H_2S .

4 Findings and conclusions

We have developed a 2-D radial reactive transport model for injection of H₂S with CO₂ in sandstone and carbonate formations, using mineralogical composition and water chemistry encountered in Songliao Basin of China, and Ohio of USA. Major findings and conclusions from simulations are summarized as follows:

(1) The preferential dissolution of H₂S gas into formation water (compared with CO₂ gas) results in the delayed breakthrough of H₂S gas, and the separation between CO₂ and H₂S gases at the moving front. Injected CO₂ gas moves faster than H₂S gas. More H₂S contains in the interior of the gas plume.

(2) Co-injection of H₂S reduces CO₂ solubility in comparison with CO₂ only case. However, the preferential dissolution of H₂S can enhance CO₂ dissolution at the gas moving front.

(3) Co-injection of H₂S with CO₂ in the sandstone formation causes the precipitation of pyrite through the interactions between the dissolved H₂S and Fe²⁺ from the dissolution of Fe-bearing minerals. Precipitation of pyrite reduces ankerite precipitation in the co-injection case, thus the mineral trapping of CO₂.

(4) In general, sandstone formations are more favorable for CO₂ mineral trapping than carbonate formations. The presence of Fe-bearing siliciclastic and/or carbonate minerals in geological formations can significantly promote the H₂S dissolution through precipitation of sulfide minerals, increasing H₂S mineral trapping.

The range of problems concerning water-rock-gas interactions is very broad. The present simulation results and conclusions are specific to the conditions and parameters considered. The “numerical experiments” presented here give a detailed view of the dynamical interplay between coupled hydrologic and chemical processes, albeit in an approximate fashion. A critical evaluation

of modeling results can provide useful insight into the spatial and temporal evolution of injected CO₂ and H₂S, and associated formation alteration in typical sandstone and carbonate formations, and better understand the behavior and effect of impurity-H₂S in the CO₂ stream.

Acknowledgements

The authors would like to thank two anonymous reviewers and the Associate Editor for their constructive comments and suggestions during the review process, which greatly improve the quality of the paper. The first author (Wei Zhang) was supported by the China Scholarship Council (CSC) and by National Natural Science Foundation of China (NSFC, No. 40872158). The second author (Tianfu Xu) was supported by the Zero Emission Research and Technology project (ZERT), of the U.S. Department of Energy under Contract No. DE-AC02-05CH11231 with Lawrence Berkeley National Laboratory. The third author (Yilian Li) was supported by the National Natural Science Foundation of China (NSFC, Nos. 40672168 and 40872158) and the Global Climate and Energy Project (GCEP, subcontract: 2384638-43106-A). The support provided by Lawrence Berkeley National Laboratory during a visit of Wei Zhang to Berkeley is also acknowledged.

Appendix A: hydrogeological parameters, and mineral and water chemical compositions

In the present paper, we used the same hydrogeological parameters (Table A1) as those used in the research in the Songliao Basin of China [Zhang et al., 2009]. Two types of (initial) mineralogical compositions (Table A2) were used, sandstone from Zhang et al. [2009] and carbonate from Zerai et al. [2006]. The initial aqueous solution compositions (Table A3) for different mineralogical compositions were obtained by batch geochemical modeling.

Appendix B: kinetic rate law for mineral dissolution and precipitation

A general kinetic rate law for mineral dissolution and precipitation is used [Lasaga et al., 1994; Steefel and Lasaga., 1994]

$$r_m = \pm k(T)_m A_m \left| 1 - \left(\frac{Q_m}{K_m} \right)^\theta \right|^\eta \quad (\text{B.1})$$

where m is the kinetic mineral index, r_m is the dissolution/precipitation rate (positive values indicate dissolution, negative values indicate precipitation), $k(T)_m$ is the rate constant depending on the temperature (mol/m² s), T is the absolute temperature, A_m is the specific reactive surface area per kg water, K_m is the equilibrium constant for the mineral-water reaction written for the destruction of one mole of mineral m , and Q_m is the corresponding ion activity product. The parameters θ and η are two positive numbers determined by experiments; usually, but not always, they are taken to be equal to 1 (like in the present work).

For many minerals the kinetic rate constant $k(T)$ can be summed from three mechanisms (Lasaga et al., 1994; Palandri and Kharaka., 2004):

$$k(T) = k_{25}^{nu} \exp \left[\frac{-E_a^{nu}}{R} \left(\frac{1}{T} - \frac{1}{298.15} \right) \right] + k_{25}^H \exp \left[\frac{-E_a^H}{R} \left(\frac{1}{T} - \frac{1}{298.15} \right) \right] \alpha_H^{n_H} + k_{25}^{OH} \exp \left[\frac{-E_a^{OH}}{R} \left(\frac{1}{T} - \frac{1}{298.15} \right) \right] \alpha_{OH}^{n_{OH}} \quad (\text{B.2})$$

where superscripts and subscripts nu , H , and OH indicate neutral, acid and base mechanisms, respectively, E_a is the activation energy, k_{25} is the rate constant at 25 °C, R is the gas constant (8.31 J/mol K), and T is the absolute temperature, α is the activity of the species, and n is a power term (constant). Notice that parameters θ and η (see equation (B.1)) are assumed to be the same for each mechanism. For all minerals it is assumed that the precipitation rate equals the dissolution rate.

Appendix C: parameters for calculating kinetic rate of minerals in the modeling studies

Parameters for calculating kinetic rate of minerals are given in Table C.1. Calcite and anhydrite were assumed to react with aqueous species at local equilibrium because their reaction rates are typically quite rapid. The dissolution and precipitation of other minerals are kinetically controlled. Rate law parameters for kaolinite, illite, chlorite, albite-low, oligoclase, K-feldspar, magnesite, and dolomite were taken from *Palandri and Kharaka* [2004], who compiled and fitted experimental data reported by many investigators. The detailed list of the original data sources is given in *Palandri and Kharaka* [2004]. Chalcedony kinetic data were referred to *Tester et al.* [1994]. Illite kinetic data was set to those of smectite. Siderite kinetic data were from *Steefel* [2001]. Ankerite and dawsonite kinetic data were set to those of siderite.

Mineral reactive-surface areas (the second column of Table C.1) are based on the work of *Sonnenthal et al.* [2005], and were calculated assuming a cubic array of truncated spheres constituting the rock framework. The larger surface areas for clay minerals (kaolinite, illite and smectite) are due to smaller grain sizes. In conformity with *White and Peterson* [1990] and *Zerai et al.* [2006], a surface roughness factor of 10 is incorporated and defined as the ratio of the true (BET)

surface area to the equivalent geometric surface area. Interaction with the minerals is generally expected to occur only at selective sites of the mineral surface, and the actual reactive surface area could be between one and three orders of magnitude less than the surface roughness-based surface area [Lasaga., 1995; Zerai *et al.*, 2006]. The difference is attributed to the fact that only part of the mineral surface is involved in the reaction due to coating or armoring, a small area exposed to the brine, and channeling of the reactive fluid flow. To account for these effects, the actual reactive surface areas given in Table C.1 are decreased by two orders of magnitude from the surface roughness-based surface areas. The reactive surface areas used here for most minerals are similar to those of Zerai *et al.*, [2006], who used a surface area of 10 cm²/g for all minerals.

If the aqueous phase supersaturates with respect to a potential secondary mineral, a small volume fraction such as 1×10^{-6} is used for calculating the seed surface area for the new phase to grow. The precipitation of secondary minerals is represented using the same kinetic expression as that for dissolution. However, because precipitation rate data for most minerals are unavailable, parameters for neutral pH rates only, as given in Table C.1, were employed to describe precipitation. Multiple kinetic mechanisms for precipitation can be specified in an input file of the TOUGHREACT program, should such information become available.

REFERENCES

- Allen, D. E., B. R. Strazisar, Y. Soong, and S. W. Hedges (2005), Modeling carbon dioxide sequestration in saline aquifers: Significance of elevated pressures and salinities, *Fuel Process. Technol.*, 86, 1569-1580, doi:10.1016/j.fuproc.2005.01.004.
- Bachu, S., D. B. Bennion, M. Pooladi-Darvish, and H. Hong (2009a), Factors affecting the chromatographic partitioning of CO₂ and H₂S injected into a water-saturated porous medium, *Energy Procedia*, 1, 3165-3172, doi:10.1016/j.egypro.2009.02.099.
- Bachu, S., and D. B. Bennion (2009), Chromatographic partitioning of impurities contained in a CO₂ stream injected into a deep saline aquifer: Part 1. Effect of gas composition and in situ conditions, *Int. J. Greenhouse Gas Control*, 3, 458-467, doi:10.1016/j.ijggc.2009.01.001.
- Bachu, S., W. D. Gunter, and E. P. Perkins (1994), Aquifer disposal of CO₂: Hydrodynamic and mineral trapping, *Energy Convers. Manage.*, 35, 269-279, doi:10.1016/0196-8904(94)90060-4.
- Bachu, S., and W. D. Gunter (2004), Acid-gas injection in the Alberta basin, Canada: A CO₂-storage experience. *Geol. Soc. Spec. Publ.*, 233, 225-234, doi:10.1144/GSL.SP.2004.233.01.15.
- Bachu, S., and W. D. Gunter (2005), Overview of acid-gas injection operations in Western Canada, paper presented at 7th International Conference on Greenhouse Gas Control Technologies, Elsevier Science Ltd., Oxford, United Kingdom, 443-448, doi:10.1016/B978-008044704-9/50045-8.
- Bachu, S., J. M. Nordbotten, and M. A. Celia (2005), Evaluation of the spread of acid-gas plumes injected in deep saline aquifers in western Canada as an analogue for CO₂ injection into continental sedimentary basins, paper presented at 7th International Conference on Greenhouse Gas Control Technologies, Elsevier Science Ltd., Oxford, United Kingdom, 479-487, doi:10.1016/B978-008044704-9/50049-5.
- Bachu, S., M. Pooladi-Darvish, and H. Hong (2009b), Chromatographic partitioning of impurities (H₂S) contained

- in a CO₂ stream injected into a deep saline aquifer: Part 2. Effects of flow conditions, *Int. J. Greenhouse Gas Control*, 3, 468-473, doi:10.1016/j.ijggc.2009.01.002.
- Battistelli, A (2008), Modeling multiphase organic spills in coastal sites with TMVOC V.2.0, *Vadose Zone J.*, 7, 316-324, doi:10.2136/vzj2006.0119.
- Crandell, L. E., B. R. Ellis, and C. A. Peters (2010), Dissolution potential of SO₂ co-injected with CO₂ in geologic sequestration, *Environ. Sci. Technol.*, 44, 349-355, doi:10.1021/es902612m.
- Ellis, B. R., L. E. Crandell, and C. A. Peters (2009), Limitations for brine acidification due to SO₂ co-injection in geologic carbon sequestration, *Int. J. Greenhouse Gas Control*, doi:10.1016/j.ijggc.2009.11.006, in press.
- Gentzis, T. (2000), Subsurface sequestration of carbon dioxide-an overview from an Alberta (Canada) perspective, *Int. J. Coal Geol.*, 43, 287-305, doi:10.1016/S0166-5162(99)00064-6.
- Gough, C. (2008), State of the art in carbon dioxide capture and storage in the UK: An experts' review, *Int. J. Greenhouse Gas Control*, 2, 155-168, doi:10.1016/S1750-5836(07)00073-4.
- Gunter, W. D., E. H. Perkins, and I. Hutcheon (2000), Aquifer disposal of acid gases: Modeling of water-rock reactions for trapping of acid wastes, *Appl. Geochem.*, 15, 1085-1095, doi:10.1016/S0883-2927(99)00111-0.
- Gunter, W.D., A. Pratt, B. E. Buschkuehle, and E.H. Perkins (2005) Acid gas injection in the Brazeau Nisku Q carbonate reservoir: Geochemical reactions as a result of the injection of an H₂S-CO₂ waste stream, paper presented at 7th International Conference on Greenhouse Gas Control Technologies, Elsevier Science Ltd., Oxford, United Kingdom, 469-477, doi: 10.1016/B978-008044704-9/50048-3.
- Hitchon, B., W. D. Gunter, T. Gentzis, and R. T. Bailey (1999), Sedimentary basins and greenhouse gases: A serendipitous association, *Energy Convers. Manage.*, 40, 825-843, doi:10.1016/S0196-8904(98)00146-0.
- Holloway, S. (2001), Storage of fossil fuel-derived carbon dioxide beneath the surface of the Earth, *Annu. Rev. Energy Environ.*, 26, 145-166, doi:10.1146/annurev.energy.26.1.145.

- Holloway, S. (2005), Underground sequestration of carbon dioxide—a viable greenhouse gas mitigation option, *Energy*, 30, 2318-2333, doi:10.1016/j.energy.2003.10.023.
- Izgec, O., B. Demiral, H. Bertin, and S. Akin (2008), CO₂ injection into saline carbonate aquifer formation I: Laboratory investigation, *Transp. Porous Med.*, 72, 1-24, doi:10.1007/s11242-007-9132-5.
- Knauss, K. G., J. W. Johnson, and C. I. Steefel (2005), Evaluation of the impact of CO₂, co-contaminant gas, aqueous fluid and reservoir rock interactions on the geologic sequestration of CO₂, *Chem. Geol.*, 217, 339-350, doi:10.1016/j.chemgeo.2004.12.017.
- Lasaga, A.C., J. M. Soler, J. Ganor, T. E. Burch, and K. L. Nagy (1994), Chemical weathering rate laws and global geochemical cycles, *Geochim. Cosmochim. Ac.*, 58, 2361-2386, doi:10.1016/0016-7037(94)90016-7.
- Lasaga, A. C. (1995), Fundamental approaches in describing mineral dissolution and precipitation rates, *Chemical Weathering Rates of Silicate Minerals, Review in Mineralogy*, vol. 31, edited by A. F. White and S. L. Brantley, pp. 23-86, Mineralogical Soc. America, Washington, D. C.
- Machel, H. G. (2005), Geological and hydrogeological evaluation of the Nisku Q-Pool in Alberta, Canada, for H₂S and/or CO₂ storage. *Oil Gas Sci. Technol.*, 60, 51-65, doi:10.2516/ogst:2005005.
- Narasimhan, T. N., and P. A. Whiterspoon (1976), An integrated finite difference method for analyzing fluid flow in porous media, *Water Resour. Res.*, 12, 57-64, doi:10.1029/WR012i001p00057.
- Palandri J. L., and Y. K. Kharaka (2004), A compilation of rate parameters of water-mineral interaction kinetics for application to geochemical modeling, *Open File Rep. 2004-1068*, pp. 64, U.S. Geol. Surv., Menlo Park, Calif.
- Pruess, K., and A. Battistelli (2002), TMVOC, a numerical simulator for three-phase non-isothermal flows of multicomponent hydrocarbon mixtures in saturated–unsaturated heterogeneous media, *Rep. LBNL-49375*, Lawrence Berkeley Natl. Lab., Berkeley, Calif.

Pruess, K., C. Oldenburg, and G. Moridis (1999), TOUGH2 User's Guide, V2, *Rep. LBNL-43134*, Lawrence Berkeley Natl. Lab., Berkeley, Calif.

Pruess, K., J. García, T. Kavscek, C. Oldenburg, J. Rutqvist, C. Steefel, and T. Xu (2004), Code intercomparison builds confidence in numerical simulation models for geologic disposal of CO₂, *Energy*, 29, 1431-1444, doi:10.1016/j.energy.2004.03.077.

Sonnenthal, E., A. Ito, N. Spycher, M. Yui, J. Apps, Y. Sugita, M. Conrad, and S. Kawakami (2005), Approaches to modeling coupled thermal, hydrological, and chemical processes in the drift scale heater test at Yucca Mountain, *Int. J. Rock Mech. Min. Sci.*, 42, 698-719, doi:10.1016/j.ijrmms.2005.03.009.

Soong, Y., A. L. Goodman, J. R. McCarthy-Jones, and J. P. Baltrus (2004), Experimental and simulation studies on mineral trapping of CO₂ with brine, *Energy Convers. Manage.*, 45, 1845-1859, doi:10.1016/j.enconman.2003.09.029.

Steefel, C. I., and A. C. Lasaga (1994), A coupled model for transport of multiple chemical species and kinetic precipitation/dissolution reactions with application to reactive flow in single phase hydrothermal systems, *Am. J. Sci.*, 294, 529-592.

Steefel, C. I. (2001), CRUNCH, Lawrence Livermore Natl. Lab., Livermore, Calif.

Tester, J. W., G. W. Worley, B. A. Robinson, C. O. Grigsby, and J. L. Feerer (1994), Correlating quartz dissolution kinetics in pure water from 25 to 625°C, *Geochim. Cosmochim. Ac.*, 58, 2407-2420, doi:10.1016/0016-7037(94)90020-5.

West, J. M., J. Pearce, M. Bentham, and P. Maul (2005), Issue profile: Environmental issues and the geological storage of CO₂, *Eur. Env.*, 15, 250-259, doi:10.1002/eet.388.

White, A.F., and M. L. Peterson (1990), Role of reactive surface area characterization in geochemical models, in *Chemical modeling of aqueous systems II*, *Am. Chem. Soc. Symp. Ser.*, vol. 416, edited by D. C. Melchior and R.

- L. Bassett, pp. 461-475, ACS, Washington, D. C., doi:10.1021/bk-1990-0416.ch035.
- Xiao, Y., T. Xu, and K. Pruess (2009), The effects of gas-fluid-rock interactions on CO₂ injection and storage: Insights from reactive transport modeling, *Energy Procedia*, 1, 1783-1790, doi:10.1016/j.egypro.2009.01.233.
- Xu, T., and K. Pruess (2001), Modeling multiphase non-isothermal fluid flow and reactive geochemical transport in variably saturated fractured rocks: 1. Methodology, *Am. J. Sci.*, 301, 16-33, doi:10.2475/ajs.301.1.16.
- Xu, T., E. Sonnenthal, N. Spycher, and K. Pruess (2006), TOUGHREACT-A simulation program for non-isothermal multiphase reactive geochemical transport in variably saturated geologic media: Applications to geothermal injectivity and CO₂ geological sequestration, *Comput. Geosci.*, 32, 145-165, doi:10.1016/j.cageo.2005.06.014.
- Xu, T., J. A. Apps, K. Pruess, and H. Yamamoto (2007), Numerical modeling of injection and mineral trapping of CO₂ with H₂S and SO₂ in a sandstone formation, *Chem. Geol.*, 242, 319-346, doi:10.1016/j.chemgeo.2007.03.022.
- Yeh, G. T., and V. S. Tripathi (1991), A model for simulating transport of reactive multispecies components: Model development and demonstration, *Water Resour. Res.*, 27, 3075-3094.
- Zerai, B., B. Z. Saylor, and G. Matisoff (2006), Computer simulation of CO₂ trapped through mineral precipitation in the Rose Run Sandstone, Ohio, *Appl. Geochem.*, 21, 223-240, doi:10.1016/j.apgeochem.2005.11.002.
- Zhang, W., Y. Li, T. Xu, H. Cheng, Y. Zheng, and P. Xiong (2009), Long-term variations of CO₂ trapped in different mechanisms in deep saline formations: A case study of the Songliao Basin, China, *Int. J. Greenhouse Gas Control*, 3, 161-180, doi:10.1016/j.ijggc.2008.07.007.

Tables in this paper

Table 1. Four groups of simulations in our studies

Simulation groups	Injection scenarios	Rock types
1	CO ₂ and H ₂ S	Sandstone
2	CO ₂ only	Sandstone
3	CO ₂ and H ₂ S	Carbonate
4	CO ₂ and H ₂ S	Carbonate without siderite

Table A.1. Hydrogeological parameters used in the simulations

Parameters	Geological formation
Porosity	0.30
Horizontal permeability (m ²)	1.0×10 ⁻¹³
Vertical permeability (m ²)	0.5×10 ⁻¹³
Pore compressibility (Pa ⁻¹)	4.5×10 ⁻¹⁰
Diffusivity (m ² /s)	1.0×10 ⁻⁹
Rock grain density (kg/m ³)	2600
Formation heat conductivity (W/m °C)	2.51
Rock grain specific heat (J/kg °C)	920
Temperature (°C)	50
Pressure (bar)	120
Relative permeability model:	
Liquid (Van Genuchten)	
$k_{rl} = \sqrt{S^*} \left\{ 1 - (1 - [S^*]^{1/m})^m \right\}^2$	$S^* = (S_l - S_{lr}) / (1 - S_{lr})$
S_{lr} : residual water saturation	$S_{lr} = 0.30$
m : exponent	$m = 0.457$
Gas (Corey):	
$k_{rg} = (1 - \hat{S})^2 (1 - \hat{S}^2)$	$\hat{S} = (S_l - S_{lr}) / (S_l - S_{lr} - S_{gr})$
S_{gr} : residual gas saturation	$S_{gr} = 0.05$
Capillary pressure model (Van Genuchten):	
$P_{cap} = -P_0 ([S^*]^{-1/m} - 1)^{1-m}$	$S^* = (S_l - S_{lr}) / (1 - S_{lr})$
S_{lr} : residual water saturation	$S_{lr} = 0.00$
m : exponent	$m = 0.457$
P_0 : strength coefficient	$P_0 = 19.61$ kPa

Table A.2. Initial mineral volume fractions introduced in the model, and possible secondary mineral phases (with a zero initial volume fraction) used in the simulations

Minerals	Chemical composition	Volume fraction	
		Sandstone formation	Carbonate formation
		Songliao Basin, China	Ohio, USA
Albite~low	$\text{NaAlSi}_3\text{O}_8$	0.415	0
Calcite	CaCO_3	0.030	0.390
Chalcedony	SiO_2	0.258	0
Chlorite	$\text{Mg}_{2.5}\text{Fe}_{2.5}\text{Al}_2\text{Si}_3\text{O}_{10}(\text{OH})_8$	0.027	0
Illite	$\text{K}_{0.6}\text{Mg}_{0.25}\text{Al}_{1.8}(\text{Al}_{0.5}\text{Si}_{3.5}\text{O}_{10})(\text{OH})_2$	0.028	0
Kaolinite	$\text{Al}_2\text{Si}_2\text{O}_5(\text{OH})$	0.009	0
K-feldspar	KAlSi_3O_8	0.233	0
Alunite	$\text{KAl}_3(\text{OH})_6(\text{SO}_4)_2$	0	0
Anhydrite	CaSO_4	0	0
Ankerite	$\text{CaMg}_{0.3}\text{Fe}_{0.7}(\text{CO}_3)_2$	0	0
Ca-smectite	$\text{Ca}_{0.145}\text{Mg}_{0.26}\text{Al}_{1.77}\text{Si}_{3.97}\text{O}_{10}(\text{OH})_2$	0	0
Dawsonite	$\text{NaAlCO}_3(\text{OH})_2$	0	0
Dolomite	$\text{CaMg}(\text{CO}_3)_2$	0	0.600
Hematite	Fe_2O_3	0	0
Magnesite	MgCO_3	0	0
Na-smectite	$\text{Na}_{0.290}\text{Mg}_{0.26}\text{Al}_{1.77}\text{Si}_{3.97}\text{O}_{10}(\text{OH})_2$	0	0
Oligoclase	$\text{Ca}_{0.2}\text{Na}_{0.8}\text{Al}_{1.2}\text{Si}_{2.8}\text{O}_8$	0	0
Pyrite	FeS_2	0	0
Siderite	FeCO_3	0	0.010

Table A.3. Initial concentrations of the formation water at reservoir conditions of 50°C and 120 bars. (Iron is the sum of Fe²⁺, Fe³⁺ and their related complexes. Carbon is the sum of CO₂(aq), CH₄(aq), and their related species such as HCO₃⁻ and acetic acid(aq). Sulfur is the sum of sulfate and sulfide species. Redox reactions are set using O₂(aq))

Elements	Concentration (mol/kg H ₂ O)	
	Sandstone formation	Carbonate formation
	Songliao Basin, China	Ohio, USA
Al	0.4235×10 ⁻⁰⁹	0.9955×10 ⁻¹⁶
Carbon	0.8150×10 ⁻⁰²	0.2741×10 ⁻⁰¹
Ca	0.2977×10 ⁻⁰²	0.2636×10 ⁻⁰³
Cl	0.1710×10 ⁺⁰⁰	0.1710×10 ⁺⁰⁰
Iron	0.8915×10 ⁻⁰⁴	0.2612×10 ⁻⁰⁵
K	0.1979×10 ⁻⁰³	0.1000×10 ⁻¹⁵
Mg	0.1141×10 ⁻⁰⁴	0.1297×10 ⁻⁰¹
Na	0.1718×10 ⁺⁰⁰	0.1710×10 ⁺⁰⁰
Sulfur	0.1000×10 ⁻¹⁵	0.9983×10 ⁻¹⁶
Si	0.1800×10 ⁻⁰²	0.1000×10 ⁻¹⁵
O ₂ (aq)	0.1774×10 ⁻⁶⁶	0.1774×10 ⁻⁶⁶
pH	6.891	7.446

Table C.1. List of parameters for calculating kinetic rate of minerals. Note that: (1) all rate constants are listed for dissolution; (2) k_{25} is kinetic constant at 25°C, E_a is activation energy, and n is the power term (equation (B.2)); (3) the power terms n for both acid and base mechanisms are with respect to H^+ ; (4) for pyrite, the neutral mechanism has n with respect to $O_2(aq)$, the acid mechanism has two species involved: one n with respect to H^+ and another n with respect to Fe^{3+}

Minerals	Surface area (cm^2/g)	Parameters for kinetic rate law							
		Neutral mechanism		Acid mechanism			Base mechanism		
		k_{25} ($mol/m^2 s$)	E_a (kJ/mol)	k_{25}	E_a	$n(H^+)$	k_{25}	E_a	$n(H^+)$
Calcite	--	Equilibrium	--						
Anhydrite	--	Equilibrium	--						
Chalcedony	9.8	1.2500e-14	87.5						
Kaolinite	151.6	6.9183e-14	22.2	4.8978e-12	65.9	0.777	8.9125e-18	17.9	-0.472
Illite	151.6	1.6596e-13	35.0	1.0471e-11	23.6	0.34	3.0200e-17	58.9	-0.40
Chlorite	9.8	3.0200e-13	88.0	7.7624e-12	88.0	0.5			
Albite~low	9.8	2.7542e-13	69.8	6.9183e-11	65.0	0.457	2.5119e-16	71.0	-0.572
Oligoclase	9.8	1.4451e-12	69.8	2.1380e-10	65.0	0.457			
K-feldspar	9.8	3.8905e-13	38.0	8.7096e-11	51.7	0.5	6.3096e-22	94.1	-0.823
Magnesite	9.8	4.5709e-10	23.5	4.1687e-07	14.4	1.0			
Dolomite	9.8	2.9512e-08	52.2	6.4565e-04	36.1	0.5			
Siderite	9.8	1.2598e-09	62.76	6.4565e-04	36.1	0.5			
Dawsonite	9.8	1.2598e-09	62.76	6.4565e-04	36.1	0.5			
Ankerite	9.8	1.2598e-09	62.76	6.4565e-04	36.1	0.5			
Na-smectite	151.6	1.6596e-13	35.0	1.0471e-11	23.6	0.34	3.0200e-17	58.9	-0.40
Ca-smectite	151.6	1.6596e-13	35.0	1.0471e-11	23.6	0.34	3.0200e-17	58.9	-0.40
Hematite	12.87	2.5119e-15	66.2	4.0738e-10	66.2	1.0			
Alunite	9.8	1.0000e-12	57.78				1.0000e-12	7.5	-1.00
Pyrite	12.87	$k_{25}=2.8184e-5$ $E_a=56.9$ $n(O_2(aq))=0.6$		$k_{25}=3.024e-8$ $E_a=56.9$ $n(H^+)=-0.5, n(Fe^{3+})=0.5$					

Figures in this paper

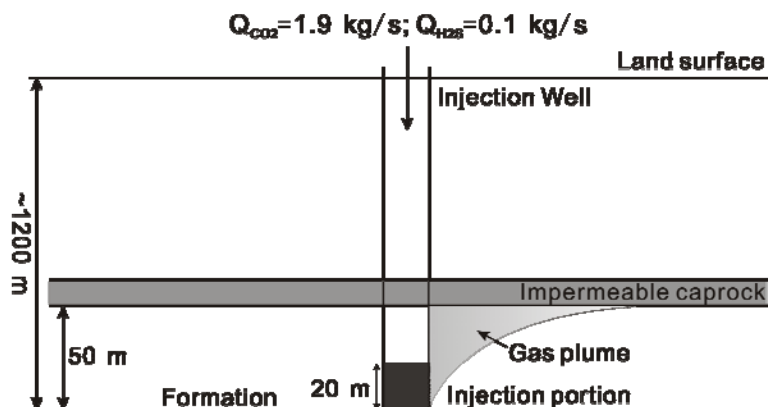


Figure 1. Schematic representation for the 2-D well flow model for the co-injection of H₂S with CO₂ in a formation [Modified from Zhang *et al.*, 2009].

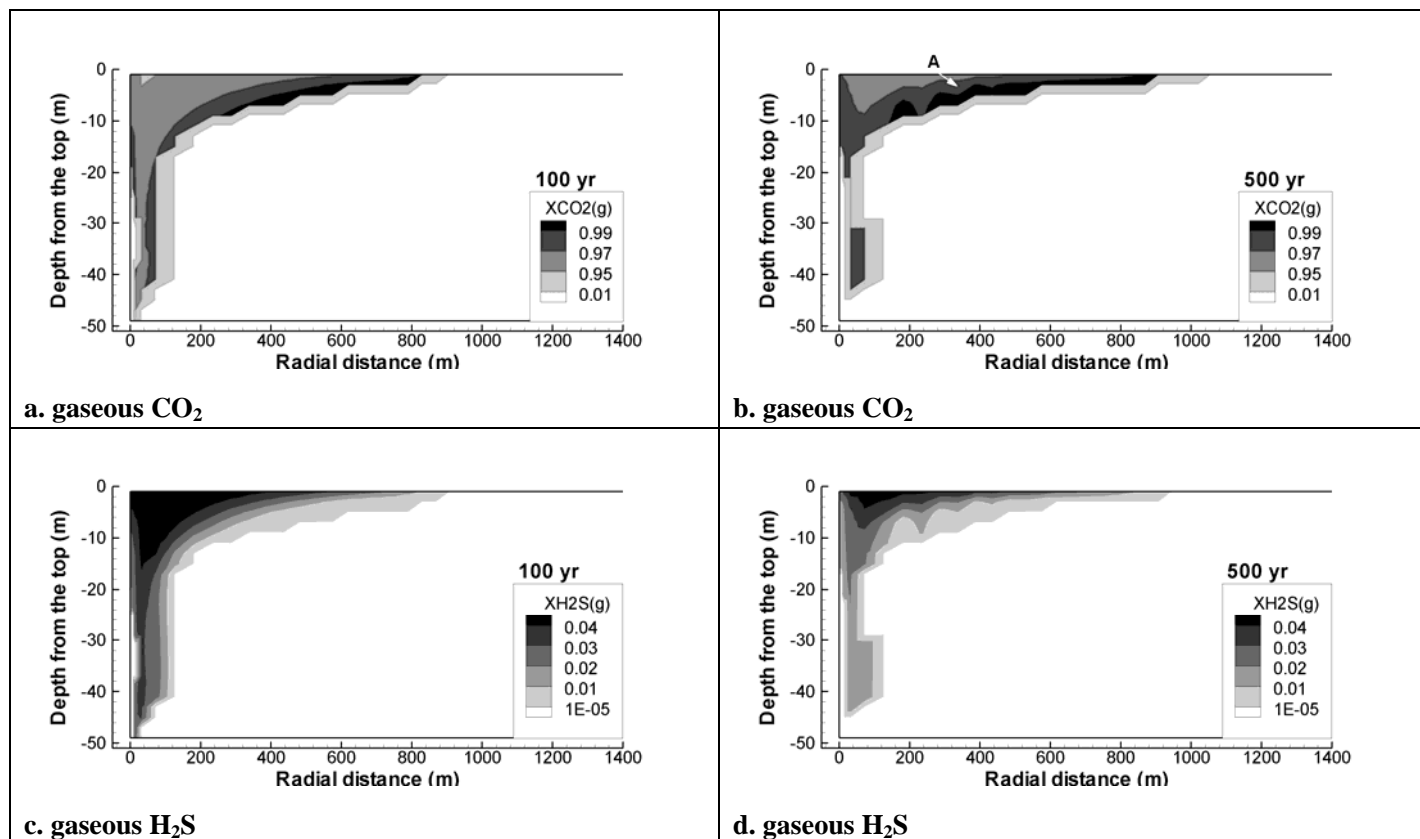


Figure 2. Spatial distribution of mass fraction of CO₂ (a and b) and H₂S (c and d) in gas phase obtained from case of H₂S with CO₂ in sandstone formation after 100 and 500 years.

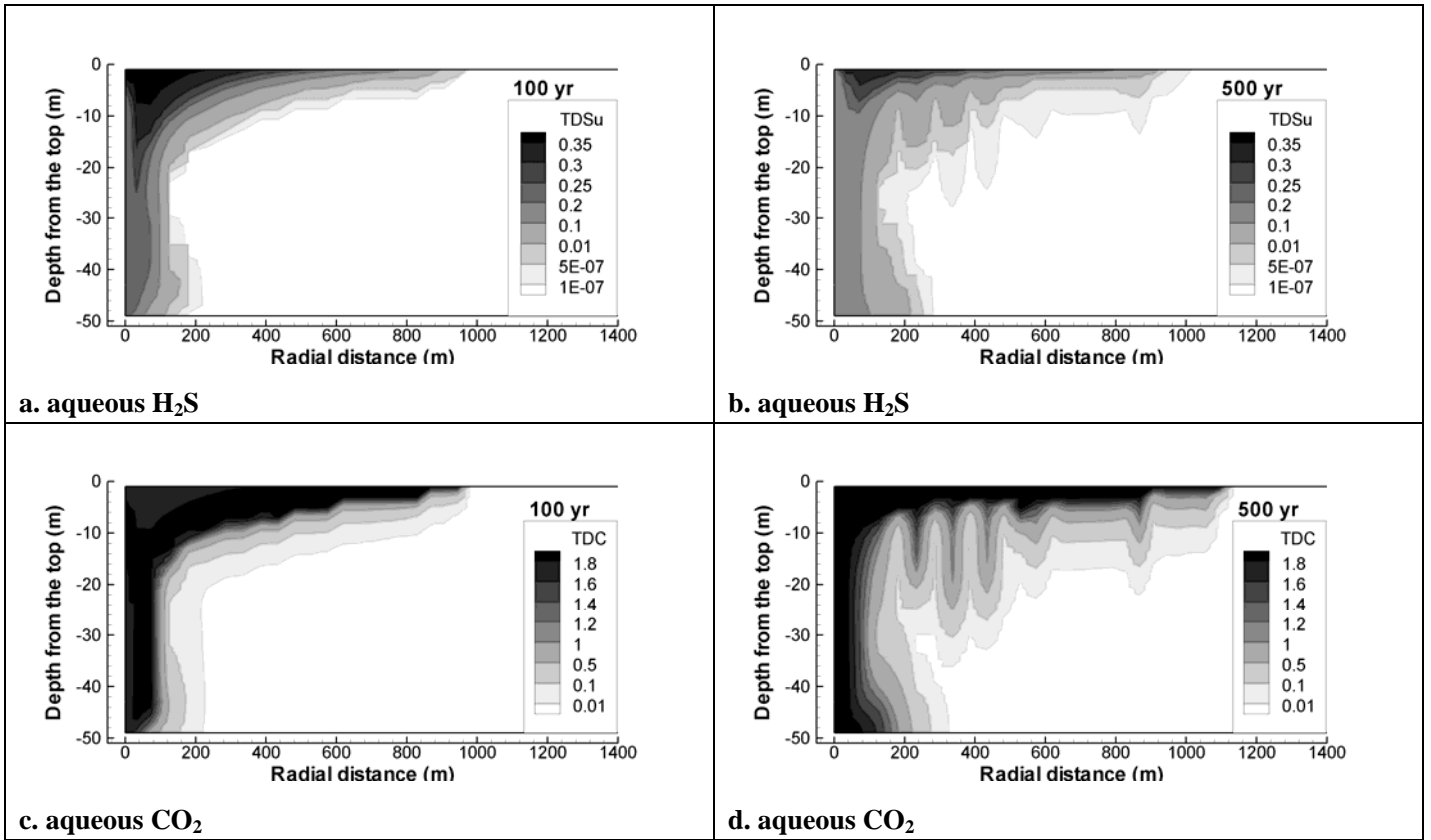


Figure 3. Spatial distribution of concentration (unit is mol/kg H₂O) of total dissolved sulfur (a and b) and carbon (c and d) obtained from case of H₂S with CO₂ in sandstone formation after 100 and 500 years.

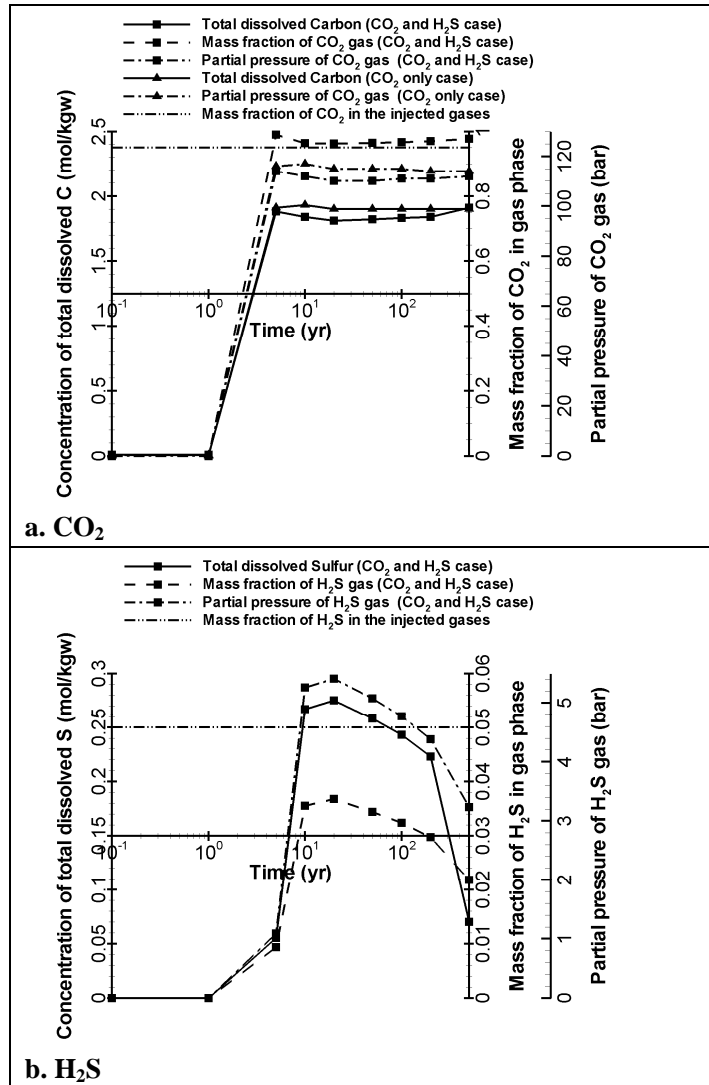


Figure 4. Changes in total dissolved carbon and sulfur, mass fraction of CO₂ and H₂S in gas phase, and partial pressure of CO₂ and H₂S with time in sandstone and carbonate formations for point A (see Figure 2b).

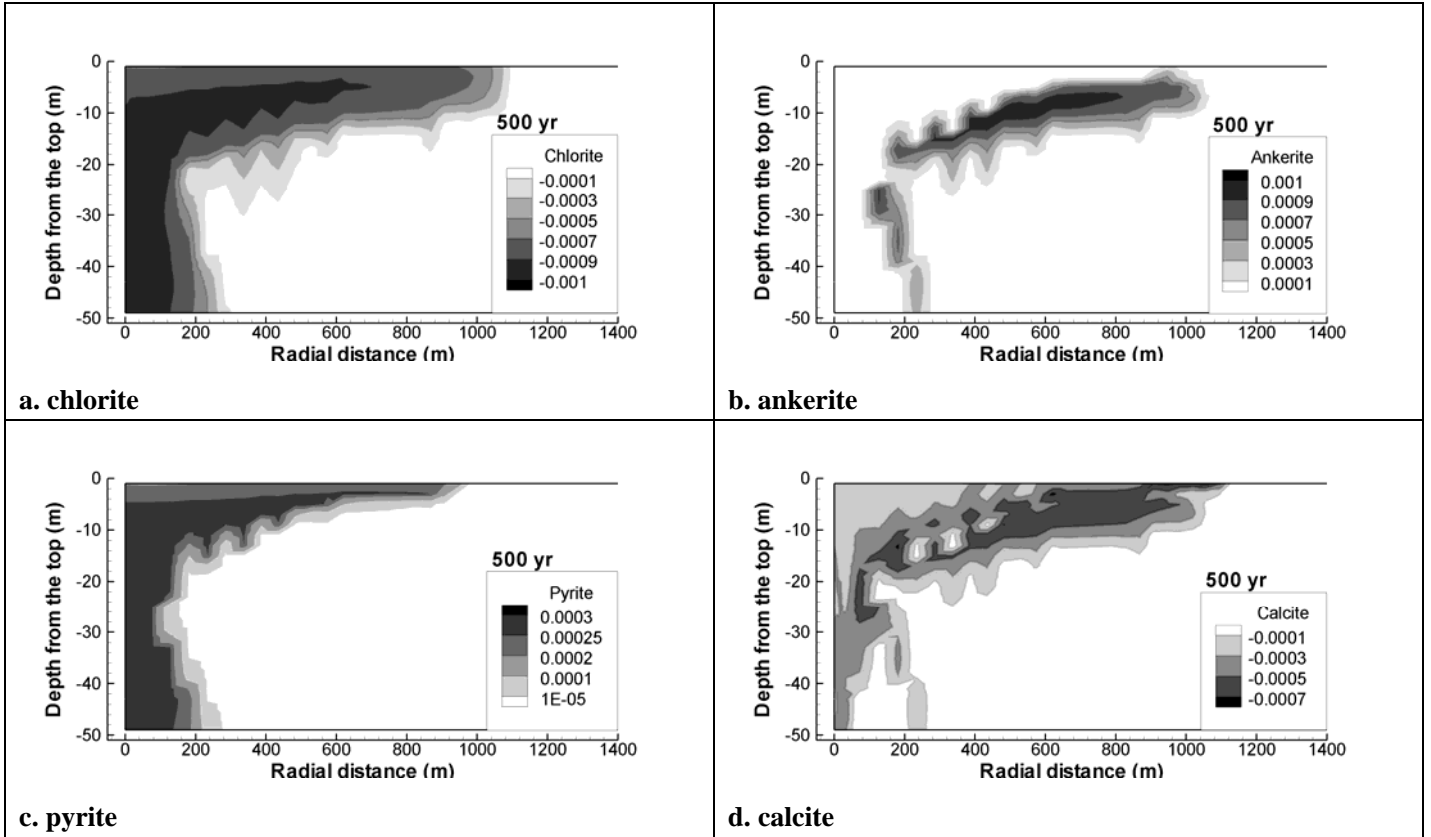


Figure 5. Spatial distribution of change of (a) chlorite, (b) ankerite, (c) pyrite, and (d) calcite obtained from case of H_2S with CO_2 in sandstone formation after 500 years (unit for minerals is change in volume fraction; positive values indicate precipitation, and negative values indicate dissolution).

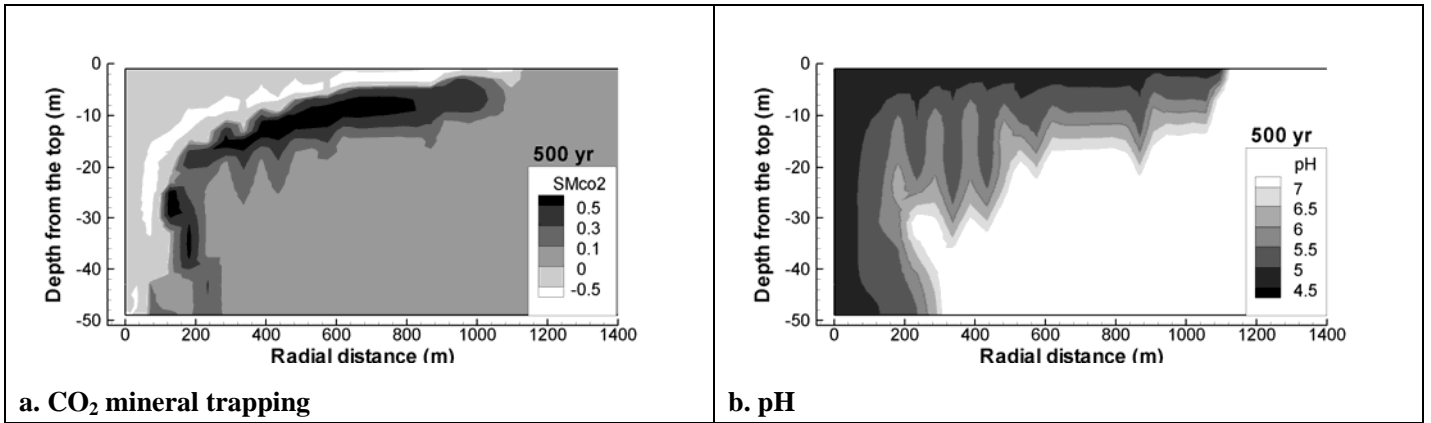


Figure 6. Spatial distribution of (a) CO_2 mineral trapping (in kg of CO_2 per m^3 medium) and (b) pH value obtained from case of H_2S with CO_2 in sandstone formation after 500 years.

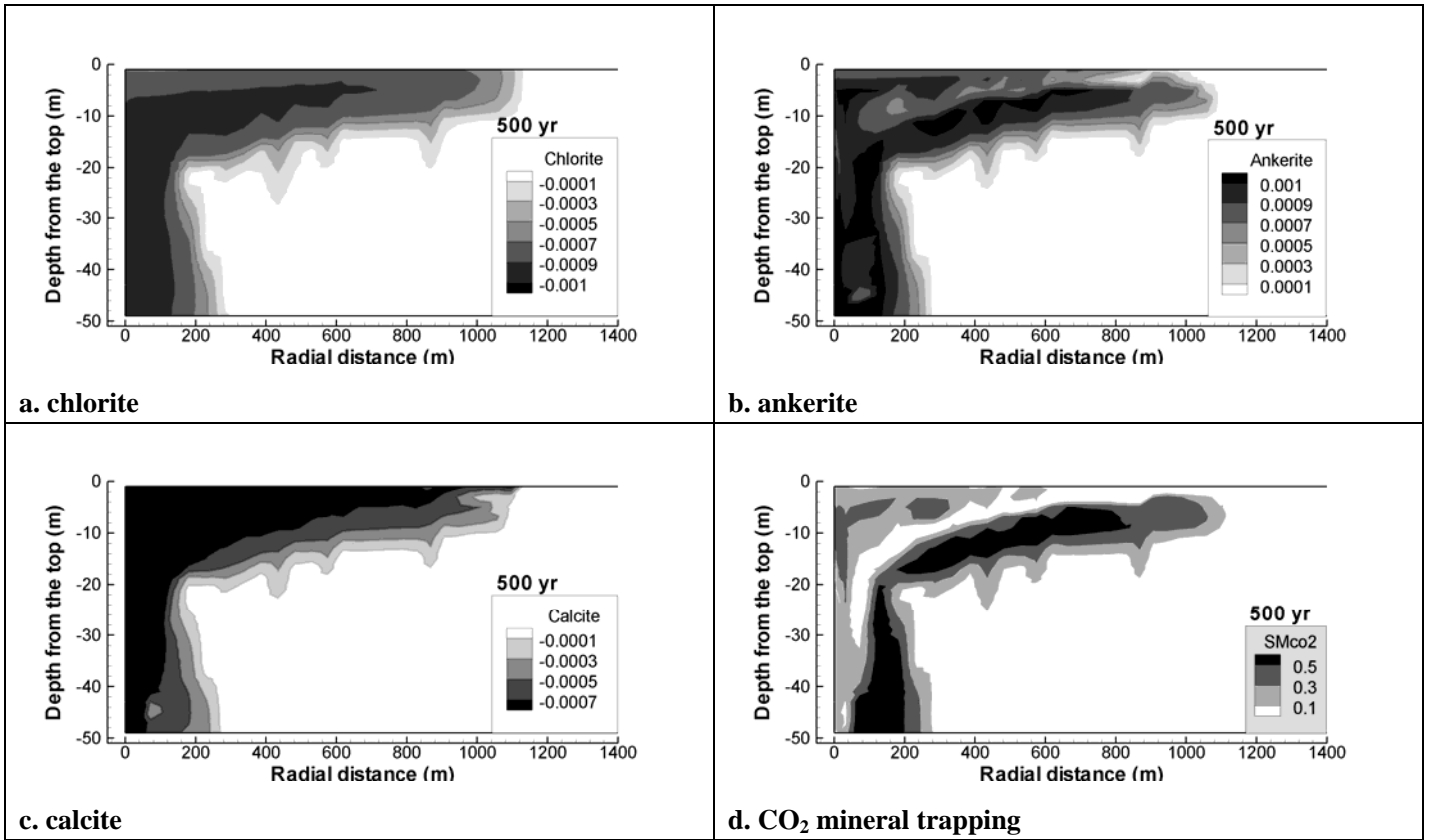


Figure 7. Spatial distribution of change of (a) chlorite, (b) ankerite, (c) calcite and (d) CO₂ mineral trapping obtained from case of CO₂ only in sandstone formation after 500 years.

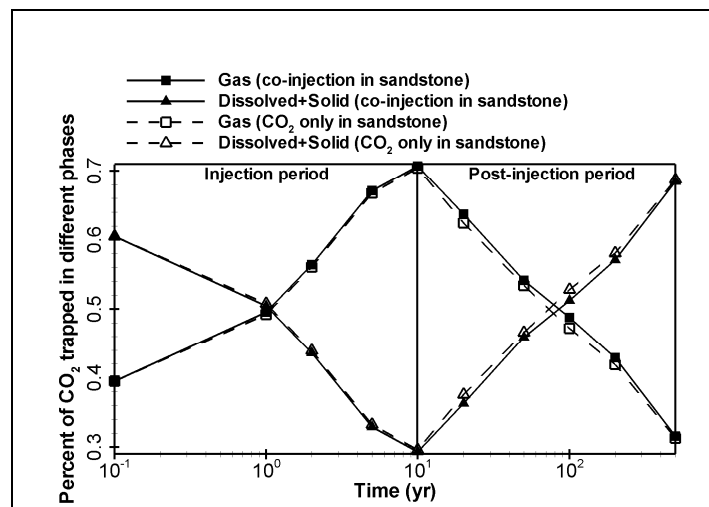


Figure 8. Comparison of time evolution of injected CO₂ in different trapping mechanisms obtained from cases of H₂S with CO₂ and CO₂ only in sandstone formations.

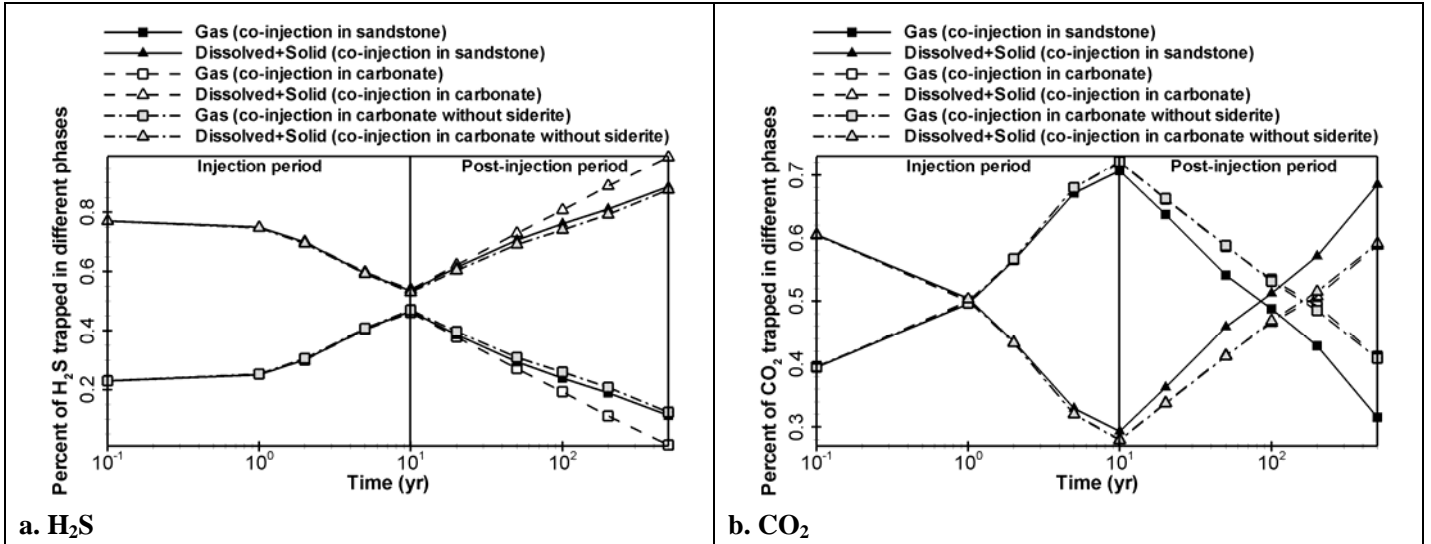


Figure 9. Comparison of time evolution of injected H₂S (a) and CO₂ (b) in different trapping mechanisms obtained from cases of H₂S with CO₂ in sandstone, and carbonate with and without siderite formations.

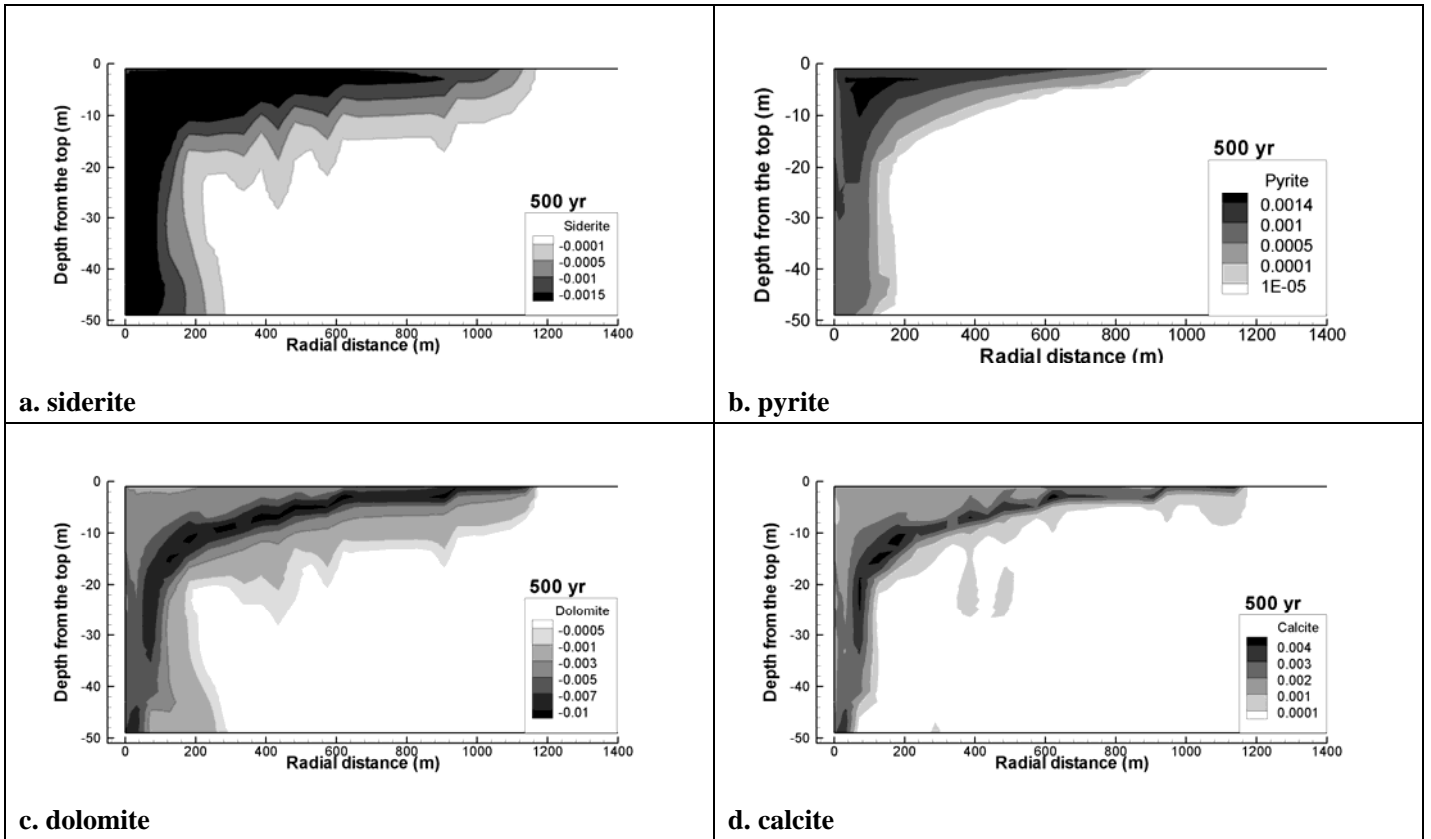


Figure 10. Spatial distribution of change of (a) siderite, (b) pyrite, (c) dolomite, and (d) calcite obtained from case of H_2S with CO_2 in carbonate formation after 100 and 500 years.

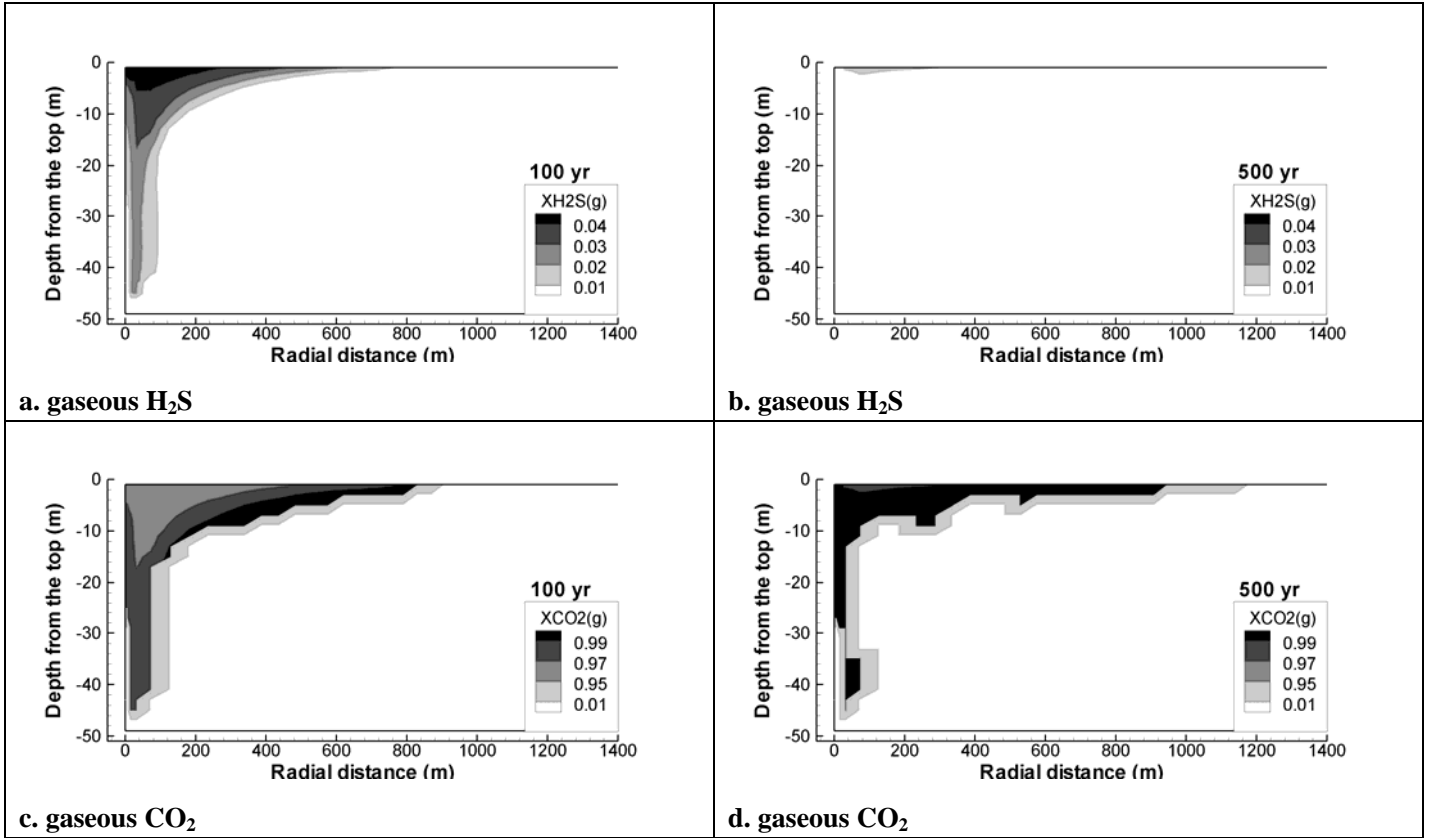


Figure 11. Spatial distribution of mass fraction of H₂S (a and b) and CO₂ (c and d) in gas phase obtained from case of H₂S with CO₂ in carbonate formation after 100 and 500 years.

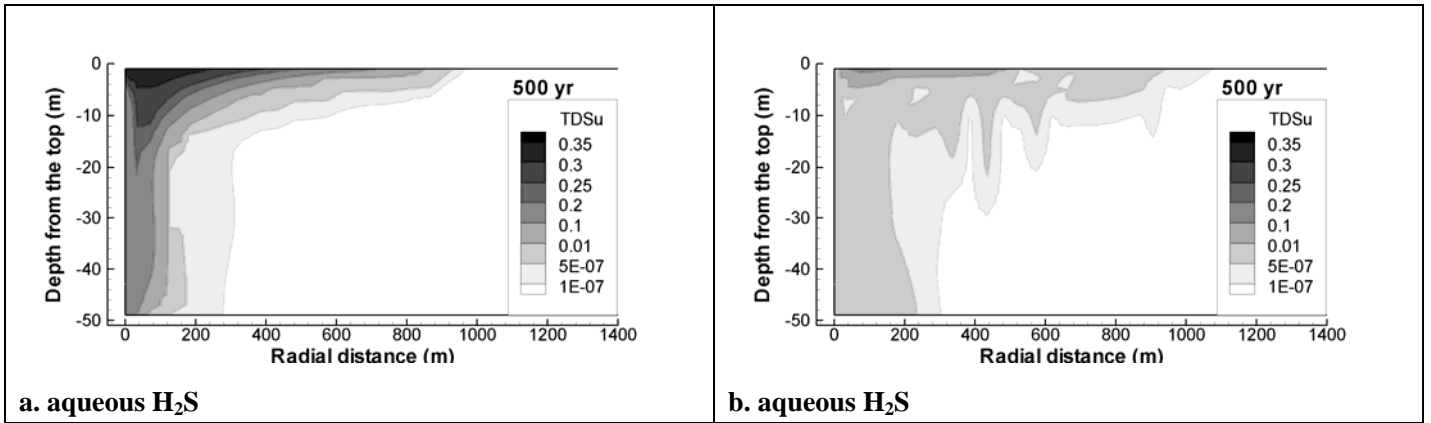


Figure 12. Spatial distribution of concentration (unit is mol/kg H₂O) of total dissolved sulfur (a and b) obtained from case of H₂S with CO₂ in carbonate formation after 100 and 500 years.

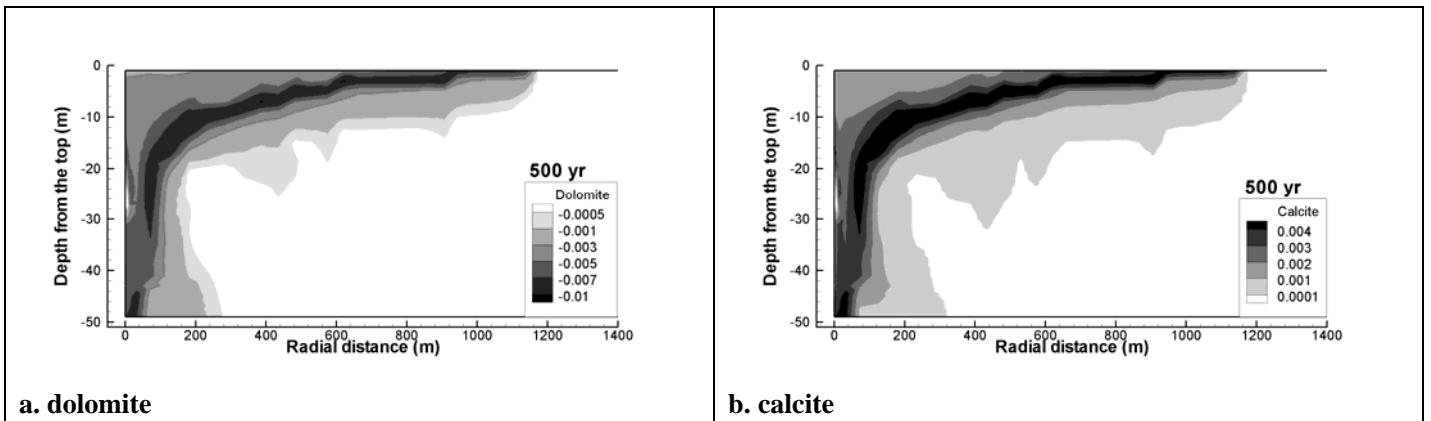


Figure 13. Spatial distribution of change of (a) dolomite and (d) calcite obtained from the sensitivity simulation after 100 and 500 years.

DISCLAIMER

This document was prepared as an account of work sponsored by the United States Government. While this document is believed to contain correct information, neither the United States Government nor any agency thereof, nor The Regents of the University of California, nor any of their employees, makes any warranty, express or implied, or assumes any legal responsibility for the accuracy, completeness, or usefulness of any information, apparatus, product, or process disclosed, or represents that its use would not infringe privately owned rights. Reference herein to any specific commercial product, process, or service by its trade name, trademark, manufacturer, or otherwise, does not necessarily constitute or imply its endorsement, recommendation, or favoring by the United States Government or any agency thereof, or The Regents of the University of California. The views and opinions of authors expressed herein do not necessarily state or reflect those of the United States Government or any agency thereof or The Regents of the University of California.

Ernest Orlando Lawrence Berkeley National Laboratory is an equal opportunity employer.